PHYSICAL REVIEW B VOLUME 26, NUMBER 4 15 AUGUST 1982

Ion-beam crystallography of InAs-GaSb superlattices

W. K. Chu
Department of Physics and Astronomy, The University of North Carolina, Chapel Hill, North Carolina 27514

F. W. Saris
FOM-Instotuut Voor Atoom-en Molecuulfysica, Kruislaan 407, Amsterdam, The Netherlands

C.-A. Chang, R. Ludeke, and L. Esaki
IBM Thomas J. Watson Research Center, P.O. Box 218, Yorktown Heights, New York 10598
(Received 8 February 1982)

(100)-oriented InAs-GaSb superlattices have been investigated with the use of high-energy helium backscattering and channeling. Oscillatory structure on the backscattering spectra confirm the existence of the superlattice periodicity. Channeling measurements reveal higher dechanneling along ⟨110⟩ directions than along the [100] growth direction. An interface relaxation and contraction model based on average bond-length changes at the interface is proposed and discussed.

I. INTRODUCTION

Man-made superlattices consist of alternating layered structures created artificially by periodically depositing two different semiconductors. This kind of modulated structure is of fundamental interest because of the occurrence of quantum-mechanical phenomena for superlattice periods comparable to the electron mean free path. Both negative differential resistance and high-frequency Bloch oscillations in a superlattice have been predicted.[1] Theoretical considerations on electron transport and optical properties have been developed as well. Synthetic modulated semiconductor superlattices are of technological importance in the development of materials for electronic applications.

Molecular-beam epitaxy (MBE)[2,3] was recognized as the most promising technique in the fabrication of multilayered heterojunction superlattices. MBE allows a relatively low-growth temperature which reduces the diffusion at interfaces, and its slow growth rates make the control of layer thickness possible down to the order of a single atomic layer. Details of the fabrication of GaAs-$Ga_{1-x}Al_xAs$ and $In_{1-x}Ga_xAs$-$GaSb_{1-y}As_y$ superlattice have been discussed and reviewed elsewhere.[4–8]

For structural information of the GaAs-$Ga_{1-x}Al_xAs$ superlattices, the most informative method has been x-ray scattering. Compositional variations have been demonstrated by Auger electron spectroscopy[9] and by ion backscattering.[10] The x-ray technique cannot, however, be applied to $In_{1-x}Ga_xAs$ and $GaSb_{1-y}As_y$ superlattices because the scattering coefficients of InAs and GaSb are nearly identical. Although Auger electron spectroscopy can provide concentration profiles, no crystalline structure information can be deduced by this technique. We have previously demonstrated that from ion backscattering and channeling experiments, information regarding the periodicity and stoichiometry of the superlattices and their interface structures can be obtained.[11] In this paper we will elaborate on our backscattering and channeling observation of InAs-GaSb superlattices.

II. SAMPLE PREPARATION

The superlattice samples were made in an MBE growth system which has several separate effusion cells containing elemental sources of the constituents In, Ga, Sb, and As. (100)-oriented GaAs and GaSb wafers were used for substrates. The substrate temperature during growth ranged between 450–600 °C. Initially InAs-GaSb samples were grown on GaAs substrates. The growth was sometimes preceded by a graded buffer layer. This buffer layer consisted of several thin layers of $In_{1-x}Ga_xAs$, of which the In concentration was gradually increased in order to compensate for the 7% lattice constant difference between the superlattice and the GaAs substrate. In our observation, however, none of the samples grown on a GaAs substrate gave satisfactory results. Therefore, we

will discuss only results for superlattices grown on GaSb.

Superlattice samples were grown on [100]-oriented GaSb substrates by periodically shuttering the beams of In and As or Ga and Sb from the effusion cells.[7] *In situ* high-energy electron diffraction measurements exhibited an instant change of streaked patterns at the start of the heteroepitaxy, indicating smooth and abrupt interfaces. The thicknesses of InAs and GaSb layers were adjusted by controlling the duration the sample surface was exposed to a given pair of elemental beams. The following different thicknesses of InAs-GaSb superlattice samples were prepared for this analysis: (50,50 Å), (90,90 Å), (220,240 Å), (410,410 Å), (1000,1000 Å), and (3000,3000 Å). In all cases, the total number of periods was sufficiently large to give at least a 1 μm thick superlattice. The size of the sample was typically 12×12 mm^2. Detailed studies of sample preparation and substrate effects on the lattice constants have been reported elsewhere.[7,8,12]

III. EXPERIMENTAL

A. Backscattering and channeling method

Ion-beam analysis, especially Rutherford backscattering and channeling, has been frequently applied in material analyses. Detailed experimental methods and physical principles of backscattering and channeling have been given elsewhere.[13,14] Briefly, the analysis consists of placing a sample in a monoenergetic beam of ions of hydrogen, helium, or any other light elements. Particles backscattered from the sample as a result of the interaction of the individual projectile and the target atoms are detected and energy analyzed. The backscattering energy spectrum (backscattering yield versus energy) gives information about the composition of the sample. There are three basic concepts involved in the backscattering analysis. Each one is at the origin of a particular capability and each corresponds to a specific physical phenomenon. They are the following:

(1) The energy transfer from a projectile to a target nucleus in an elastic two-body collision leads to the concept of the kinematic factor and to the capability of mass distinction. In an elastic two-body collision, projectiles scattered from a heavy nucleus carry more energy than those scattered from a lighter nucleus.

(2) The likelihood of the occurrence of such a two-body collision is very small. However, its functional dependence on the atomic number of the target nucleus ($\propto z^2$) leads to the concept of a scattering cross section and to the capability of quantitative analysis.

(3) The projectiles are capable of penetrating deeply into the sample. Average energy losses of projectiles moving through a dense medium leads to the concept of stopping power of the medium. This provides the capability of translating an energy loss into a depth perception. The accessible depth to backscattering experiments is typically submicrometer to a few micrometers, depending on the energy and the mass of the projectile used.

Backscattering analysis provides the ability to distinguish the atomic masses of the sample and their distribution in depths; in effect, backscattering provides a mass-sensitive depth microscopy.[13,14] In practice, backscattering analysis involves the interpretation of the backscattering energy spectrum based on the above three concepts. Quite often, the effects of mass and depth differences on the backscattering energy are superimposed. Prior knowledge on the sample or independent scattering measurements at different energies or different scattering angles is needed to unravel the problem.

When the sample is a single-crystal solid and if the ion beam enters the sample in a direction parallel to a major crystalline direction, the likelihood of the backscattering occurrence is greatly reduced. This phenomenon is called channeling. Charged particles penetrating the single crystal along or near a major axis experience a collective potential produced by the rows of atoms along the axis. If the incident direction of the ion beam is nearly parallel with the string of atoms, the string potential will steer the charged particle beam forward. For this reason the channeling technique is frequently used to study crystal defects, although it is not very sensitive to defect detection, nor very specific to the nature of the defect; however, it is a very attractive and unique method for certain defect studies. For example, it provides the depth distribution of defects and is sufficiently sensitive for identifying the lattice location of impurity atoms in a host lattice. It is furthermore useful in the study of surface and interface structures, as this paper will illustrate.

B. Oscillations in the backscattering energy spectra

Backscattering and channeling measurements in this study were made with a $^4He^+$ beam from the

3-MeV Van de Graaff accelerator at the IBM Research Center. The superlattice samples were mounted on a double-axis goniometer. The ions backscattered from the target, held at room temperature, were detected with an energy resolution of 22 keV. This detector could be moved around the target to get different scattering angles. The tilt angle of the sample and the scattering angle determine the ratio of the path lengths the ion beam travels in the sample before and after scattering. This ratio influences the shape of the backscattering energy spectra. For certain experimental conditions, oscillations exist in the energy spectrum for a given sample.

Figure 1 shows backscattering spectra taken from a (100) superlattice sample with 20 periods of 410 Å InAs and 410 Å GaSb. For comparison, the backscattering spectra from a GaSb(100) single crystal are also given as dashed curves. The (100) channeling spectra are obtained by careful alignment of the sample such that the 2.23 MeV $^4He^+$ ions are incident parallel to the [100] axis. The random spectra are obtained by tilting the sample 7° with respect to the channeling beam while the sample is in constant rotation with respect to the normal of the surface. The solid-state surface barrier detector was located at 170° with respect to the incident beam direction for the spectra of Fig. 1.

The yield of the random spectrum from the GaSb single crystal shows a smooth curve with leading edge formed by the yield of $^4He^+$ scattered from Sb atoms on the surface of the crystal. He ions scattered from the lighter Ga atoms have lost 182 keV more energy than those scattered from the heavier Sb atoms due to the difference in the collision kinematics in the energy transferred to the recoiled atoms. Lighter atoms take more energy in recoil, therefore the step in the spectrum 182 keV behind the leading edge is due to the backscattering contribution from Ga atoms of GaSb.

The oscillatory nature of the backscattering yield from the superlattice sample gives clear evidence of its periodic structure. The reason for peaks and valleys may be understood from the details of Fig. 2, where a schematic of the layered structure of the superlattice sample and backscattering signals from each element at each layer are given with the height and width in proportion to the layered structure of our 410—410 Å superlattice. Since Sb is the heaviest atom of all four constituents of the superlattice, and since its top consists of 410 Å GaSb, the highest-energy peak in the spectrum is due to He^+ backscattered from Sb in this top layer.

The energy width of the schematic spectrum Sb_1 in Fig. 2 is proportional to the thickness of the first GaSb layer. This energy width is the result of energy losses of the He ions because of interactions with the target atoms while traversing into and out of the top GaSb layer. The total energy loss of the projectile in its inward path, its scattering from Sb at the first interface, and its outgoing path through the 410-Å layer of GaSb, give about a 24-keV shift from that scattered from Sb at the surface. This 24-keV width is in good agreement with the estimate based on the semiempirical energy-loss

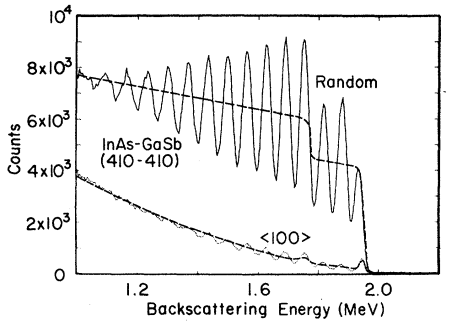

FIG. 1. Backscattering spectra for 2.23 MeV $^4He^+$ ions incident along the [100] channeling and random directions (7° off plus rotation) of an InAs-GaSb superlattice with 20 periods of 410 Å InAs and 410 Å GaSb. For comparison, backscattering measurements from a GaSb single crystal are also given as the dashed curves for both random and [100] channeling directions.

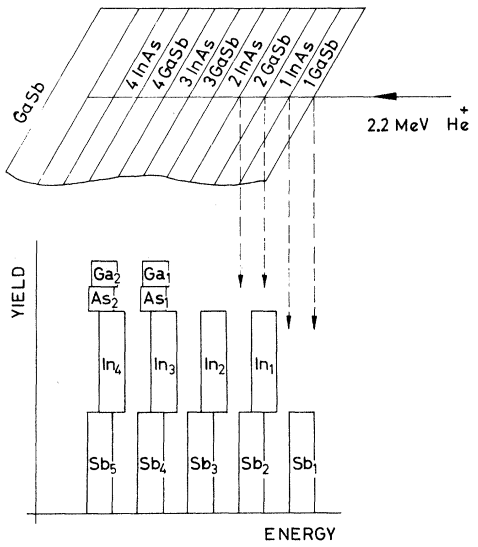

FIG. 2. Schematic representation of the origin of the oscillatory backscattering yield for the superlattice discussed in Fig. 1.

values tabulated by Ziegler.[15] The tabulation is for single elements. In our estimation, linear additivity of energy loss is assumed to give energy loss value in GaSb and a bulk density is assumed for the conversion from the thickness of the film to the number of molecules per unit area. The signal from the In at the top interface will be displaced by 15 keV from the Sb at the same depth due to the slight difference in recoil. This makes the In signal overlap with the second layer of Sb in the GaSb, which is displaced from the surface GaSb by 24 keV due to the incoming and outgoing energy loss in the first InAs layer. The addition of the In signals on top of the Sb signals will continue into the layers, which produces the oscillatory behavior of the energy spectrum for the superlattice given in Fig. 1. Therefore, the second peak in the random-spectrum from the superlattice is due to In in the first InAs layer plus Sb from the second GaSb layer. The third peak in the spectrum is due to the second InAs layer plus the third GaSb layer. The fourth and following peaks are higher again, due to the additional signals from the lighter elements, As and Ga. The mass difference between those two elements happens to be such that the difference in backscattering energy is 28.3 keV which is close to the energy loss of 25 keV for each 410-Å layer. Consequently, these signals add up. Note that Ga is lighter than As and the top layer of the superlattice is GaSb. Thus, the fourth peak of our spectrum consists of the sum of the yields due to Ga in the first GaSb layer, As in the first InAs layer, Sb in the fourth GaSb layer, and In in the third InAs layer. The fifth peak is due to Ga and As from the second GaSb and InAs layers plus Sb from the fifth GaSb and In from the fourth InAs layer, etc.

C. Computer simulation of a spectrum

Computer simulation of a random backscattering spectrum for a given sample and experimental conditions is very useful for the planning of the experiment, as well as for interpreting the measured spectra. Ziegler *et al.*[16] have written computer codes for the synthesis of backscattering spectra. In their codes, detector resolution and energy straggling can be taken into account to provide a convoluted spectrum. The result of such a computer-generated spectrum is given in Fig. 3 as a dashed curve. For comparison, the measured random spectrum given in Fig. 1 is repeated in Fig. 3. In the computer simulation, the detector resolution is

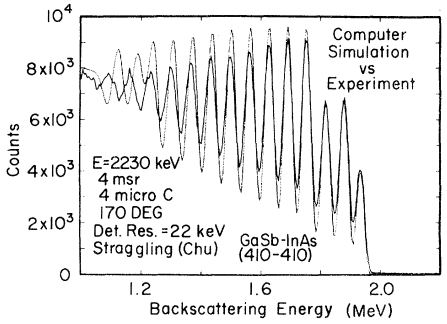

FIG. 3. Computer simulation (dotted curve) of a random backscattering spectrum from a (410, 410 Å) superlattice. The input parameters for this simulation are the following: incident He ion energy, 2.23 MeV; angle of incident 10°; detector angle, 170°; detector resolution, 22 keV; energy straggling factors based on Refs. 17 and 18; solid angle, 4 msr; total charge collection 4 μC; energy per channel, 5 keV. The experimental curve of Fig. 1 is also given as the solid curve for comparison.

assigned an experimentally obtained value of 22 keV full width at half maximum (FWHM). The values of energy straggling are assumed to follow Chu's calculation.[17,18] Isotopic shifts are included in the simulation. Other experimental conditions which are input parameters for the computer simulation are labeled in Fig. 3. The period of the superlattice is assumed to be 410−410 Å for this particular InAs-GaSb sample. Thinner or thicker layers will produce simulated spectrum out of phase with the measured spectrum. This type of simulation also produces a measurement of the layer thickness. The accuracy of this type of measurement is directly dependent on the accuracy of the stopping power information used in the simulation, and on the assumed validity of the additivity of stopping powers. We estimate that the probable error in the thickness determination is about $\pm 10\%$. The thickness value (410 Å) is reasonably close to the value of 500 Å predicted from the growth parameters. Bulk lattice parameters have been used in the conversion of layer thickness to atoms per unit area as measured by backscattering.

The oscillation of the experimental spectrum in Fig. 3 is not as strong as that of the simulated spectrum. The discrepancy between the experimental and simulated spectra in Fig. 3 can be interpreted as being due to one or several of the following reasons: First, any thickness variation from layer to layer as compared with the standard 410 Å will cause an alteration in the oscillations; second, an underestimate of the detector energy resolution and the projectile energy straggling will

make the simulated spectrum sharper; third, lateral thickness variations of a given layer over the area of the analyzing beam spot (0.2 mm^2) and interdiffusion at the interface would also produce a smearing effect. We are not able to distinguish between these possibilities. A deterioration of the solid-state detector from 22 to 27 keV (FWHM) could also produce the same amount of smearing.

In general, the agreement between the computer simulation and the measured profile is good and the simulation provides a thickness measurement of the layer and a confirmation of the stoichiometry of InAs and GaSb layers. In the deeper portion of the spectrum (lower-energy portion), damping of the oscillation is seen in both simulated and measured spectra. This damping is primarily the result of both increased energy straggling of the beam at greater depths and changes in energy loss for lower energies, such that the matching between the energy loss and kinematic difference becomes worse.

For superlattice samples with thinner or thicker layers the shape of the random spectra changes due to the change of energy loss per layer and its matching (or mismatching) of the collision kinematics. For example, Fig. 4 shows the random and [100] channeling spectra of a (50—50 Å) InAs-GaSb superlattice. The backscattering conditions are the same as that of Fig. 1 except that the incident energy is slightly higher. The oscillations are absent in Fig. 4 due to the fact that the thickness of the layer is too small to produce sufficient energy loss to match the energy shift due to the kinematic factor difference.

Figure 5 shows random and [100] channeled spectra of a (220—240 Å) InAs-GaSb superlattice.

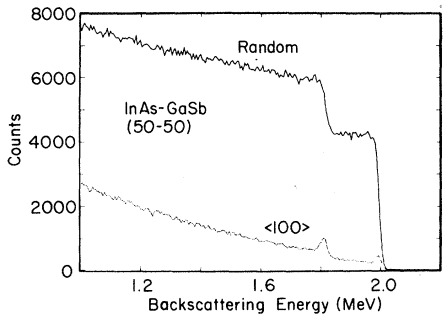

FIG. 4. Backscattering spectra for 2.272 MeV $^4He^+$ ions incident along the [100] channeling and random directions in an InAs-GaSb superlattice with 50 Å InAs and 50 Å GaSb alternating crystal layer thickness. The total thickness of the superlattice is around 1 μm, and it is epitaxially on GaSb (100) single crystal.

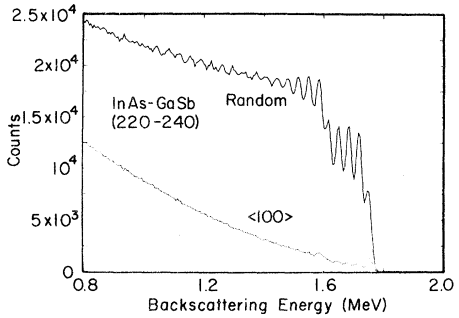

FIG. 5. Same as Fig. 4 except the thicknesses of the superlattice layers are 220 and 240 Å for InAs and GaSb, respectively. The incident energy of the helium beam is 2.005 MeV.

The oscillations on the random spectrum are not as pronounced as those in Fig. 1. As we discussed earlier, the oscillations of the backscattering spectrum are caused by the matching of total energy loss through incoming and outgoing path lengths in a layer and the recoil energy difference between Sb and In. A change of target tilt angle will change the path length of the projectile before and after scattering. A change of detector angle will change the outgoing path length after scattering, as well as the recoil energies which are a function of scattering angle. Both above-mentioned adjustments in target and/or detector geometry enable us to tune the energy spectrum for signal optimization. This type of tuning is illustrated in Fig. 6, where backscattering simulations for different target angles are calculated in order to search for the optimum conditions for a (50—50 Å) InAs-GaSb superlattice. The simulation in Fig. 6 indicates that tilting the target such that the normal of the target surface is 60° away from the incident beam does not produce oscillations at all, and the backscattering spectrum is similar to that obtained at the near normal incidence given in Fig 4. However, at an 80° tilt, a small oscillations is observed, and at 85° a large oscillation is observed in the simulated spectrum. We cannot do glancing-angle backscattering because our sample is too small (5×5 mm^2) for our beam spot under glancing-angle conditions.

For thicker samples tilting is not required for the observation of oscillation, as shown in the earlier figures. For very thick layers, such as (1000, 1000 Å) and (3000,3000 Å) superlattice, the oscillations exhibit a larger period. Figures 7 and 8 show the random and aligned spectra for 1000 and 3000 Å layers. Detailed experimental conditions are given in the figure captions.

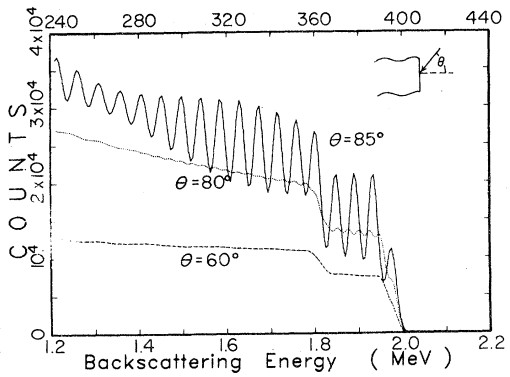

FIG. 6. Computer simulation of three random backscattering spectra from a (50, 50 Å) superlattice sample. The input parameters are the following: incident He ion energy, 2270 keV; detector angle, 170°; detector resolution, 22 keV; solid angle, 3.8 msr; total charge collected, 10 μC. The incident angle, i.e., the angle between the incident beam and the normal of the target is a variable in this figure. Three simulations are made at incident angles at 60° (dash-dot), 80° (dot), and 85° (solid curve). Large oscillations are seen only at near glancing incidence.

D. Channeling studies of superlattices

In the preceding section we have focused our attention on backscattering spectra under random directions of incidence. We have discussed the oscillations in the spectra and their thickness dependence. In this section we will concentrate on the backscattering spectra with incident beams along major channeling directions. In the channeling directions backscattering is greatly reduced. The ratio of the channeled and random backscattered intensity at a given energy loss is called the

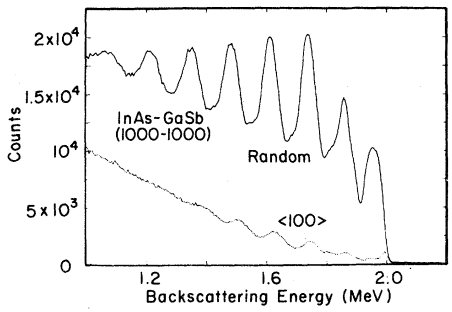

FIG. 7. Same as Fig. 4 except that the thicknesses of the superlattice layers are 1000—1000 Å. The incident beam energy is 2.272 MeV.

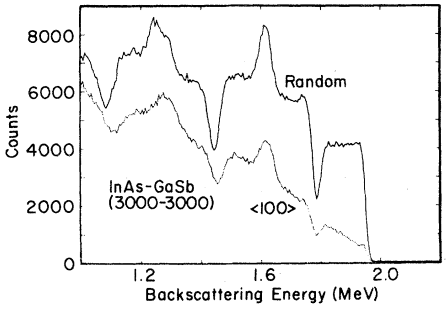

FIG. 8. Same as Fig. 4 except that the thicknesses of the superlattice layers are 3000—3000 Å. The incident beam energy is 2.23 MeV.

minimum yield $\chi_{\min}$ and is typically evaluated right behind the surface peak. In general, minimum yield can be defined at a given backscattering energy which will correspond to the minimum yield at a given depth. The increase of minimum yield at greater depth is called dechanneling, and is caused by the fact that a number of the channeled particles scatter and diverge into a nonchanneling direction with higher scattering probability. Imperfections in the crystal such as dislocations, stacking faults, clusters, or twins can produce excessive dechanneling. Quite often channeled backscattering spectra provide an indication on the quality of the crystal. The lower the intensity of the channeling spectrum as compared to the random spectrum, the lower the level of defects in the crystal. However, one has to realize that channeling is not a very sensitive method in defect analysis. For example a minimum dislocation density for detection by channeling is estimated to be 10^9- to 10^{10}-cm length of line/cm^3.

Figure 1 has shown that when the superlattice sample or the GaSb single-crystal sample is aligned along its [100] direction normal to the surface, the backscattering yields are very much reduced due to the channeling effect. In fact, except for the weak oscillatory structure in the case of the superlattice, the channeling spectra for both are almost indistinguishable. This is an indication that the superlattice has been grown in perfect epitaxial relationship to the GaSb substrate, and with a defect density below the sensitivity of the measurement. The quality of the superlattice do vary from sample to sample. By normalizing the channeled spectrum to the random spectrum, one can recognize, by comparing Figs. 1, 4, 5, 7, and 8, that the quality of the crystal given in Fig. 8 is inferior to those given in the other figures. There is an indication that

superlattices of increasing layer thickness exhibit increased dechanneling. This can be expected because thinner layers can accommodate slight lattice misfit by strain, whereas thicker ones prefer instead the formation of misfit dislocations. In general, our measurements of channeling along the [100] direction indicate that most of the superlattice samples are of good crystalline quality. However, we have consistently observed, and show results in Fig. 9, that the dechanneling rates along any one of the four ⟨110⟩ directions are much higher than those along the [100] for the same (410—410 Å) sample discussed earlier and shown in Fig. 1.

Backscattering and ⟨110⟩ channeling spectra on a (100) single crystal GaSb are also given as dashed lines for comparison. A comparison of Figs. 9 and 1 shows that for the superlattice sample, the dechanneling rate along a ⟨110⟩ direction is very much higher than for the single crystal GaSb. It was also observed that for the superlattice samples the dechanneling rate along a ⟨110⟩ is very much higher than that for the *same* sample along the [100] direction. This is contrary to the observed ⟨110⟩ vs [100] dechanneling rates for single crystal GaSb, where ⟨110⟩ dechanneling is lower.

Similar higher dechanneling yields along ⟨110⟩ directions have been observed in all InAs-GaSb superlattice samples. Figure 10 illustrates backscattering along a ⟨110⟩ for the (220—240 Å) superlattice sample discussed earlier. A comparison of Figs. 10 and 5 indicates another example of the high dechanneling observation along a ⟨110⟩ direction, as compared as the [100], for the present superlattices.

A summary of the channeling study is given in Table I where minimum yields at various depths are defined as the ratio of the channeled spectrum to the random spectrum, neglecting all oscillations. The minimum yields are measured along the [100] and ⟨110⟩ directions and the ratio of the two values is also given. The surface values given in Table I are determined immediately below the surface peaks in this spectra. The depths 1, 2, and 3 are arbitrarily defined from the energy position of the backscattering spectra and correspond to approximately 0.15-, 0.33-, and 0.5-μm depths, respectively. Incident energies for the above measurements ranged from 2.0 to 2.27 MeV. From Table I it is quite obvious that higher dechanneling is observed in all superlattice samples along the ⟨110⟩ direction. The table further shows that the ratios of minimum yield for the [100] to that for ⟨110⟩ directions is less than 1 for all superlattice samples, but that the ratio is greater than 1 for the single crystal GaSb.

For all diamond-structure single crystals, dechanneling rates along ⟨110⟩ directions are always less than those along ⟨100⟩ directions and is demonstrated for GaSb by the dashed curves in Figs. 9 and 1. This is because the packing of atoms along ⟨100⟩ directions for a diamond structure is denser than that along ⟨110⟩ directions. This leaves larger "transparent" areas for the incident ions when channeled along the ⟨110⟩ direc-

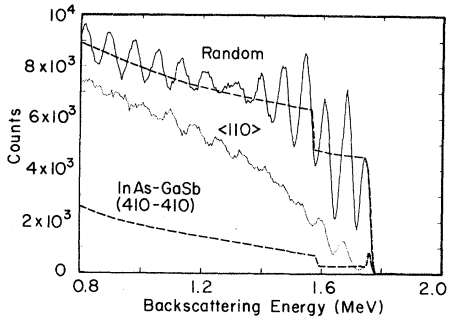

FIG. 9. Backscattering spectra for 2.23 MeV $^4He^+$ ions incident along ⟨110⟩ channeling and random direction in the same (410—410 Å) superlattice sample studied in Fig. 1. For comparison, ⟨110⟩ channeling and random spectra of a single crystal GaSb are also given as the dashed curves. Abnormally high dechanneling is observed along the ⟨110⟩ direction for the superlattice.

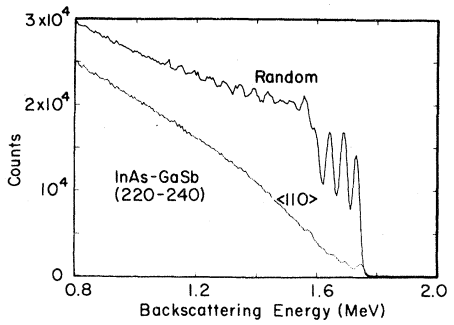

FIG. 10. Backscattering spectra for 1.99 MeV $^4He^+$ ions incident along ⟨110⟩ channeling and random direction in the same (220—240 Å) superlattice sample studied in Fig. 5. Higher dechanneling yields are observed in a ⟨110⟩ direction than are shown in the [100] direction.

TABLE I. Minimum yield for ⟨100⟩ and ⟨110⟩.

Sample No. Period Å			1	2	3	4
		GaSb	(50–50)	(200–240)	(410–410)	(1000–1000)
	⟨100⟩	7%	5%	4.6%	7%	6%
Surface	⟨100⟩	6%	11%	9.4%	13%	8%
	Ratio	1.2	0.45	0.49	0.54	0.75
	⟨100⟩	16%	12.3%	12.3%	10.2%	13%
Depth 1	⟨110⟩	10%	24%	46%	32%	16%
	Ratio	1.6	0.51	0.27	0.32	0.81
	⟨100⟩	23%	19.4%	25%	22.4%	20%
Depth 2	⟨110⟩	14%	39%	66%	58%	25%
	Ratio	1.6	0.5	0.39	0.39	0.80
	⟨100⟩	30%	27%	40%	38%	20%
Depth 3	⟨110⟩	20%	58%	79%	70%	33%
	Ratio	1.5	0.47	0.50	0.54	0.60

tions. Thus the contrary results observed on all InAs-GaSb samples are puzzling and warrant further investigations.

We have considered the possibility that certain dislocations could be the cause of the high dechanneling yield along the ⟨110⟩ directions. However, in the first place, it is difficult to conceive a type of dislocation which provides high dechanneling effects along the ⟨110⟩ but has low or no effect along the [100] growth directions. In the second place, if the high dechanneling rate along ⟨110⟩ directions is caused by some special kind of dislocations, then the dechanneling rate will be related to the incident energy of the analyzing beam. A study of the energy dependence of the dechanneling rate should shed some light on the nature of the "defect" of the superlattice samples studied here. We will present the result in the next section.

E. Energy dependence of dechanneling

As mentioned earlier, backscattering and channeling are not very sensitive in detecting crystal defects. Nevertheless, defects cause and increase scattering and dechanneling of the ion beam. Therefore, an accurate interpretation of the dechanneling data requires knowing the nature of the defect. This defeats the purpose of using channeling to analyze the defect in our case. However, certain defect models can always be assumed and their effect on the dechanneling results predicted. Agreement, or lack thereof, with experimental result can then be used as an indicattion of the model's validity.

One of the earlier approaches in the development of channeling application on defect characterization was to study defective samples which were well characterized by independent measurements such as transmission electron microscopy, and to see how channeling measurements respond to a known type of defect. Regarding dislocations, Foti *et al.*[19] observed that the amount of dechanneling in a Zn-implanted Al single crystal is proportional to the square root of the energy of the impinging ion beam. Their results are in good agreement with a distortional steering model given by Quere.[20]

Dechanneling is defined by the increase of minimum yield χ per unit distance $d\chi/dx$, which itself is a function of depth x. The evaluation of dechanneling for spectra taken at different energies is further complicated by the fact that the depth scale changes with projectile energy. Therefore $d\chi/dx$ cannot be seen from the slope of the channeled spectrum, which is a measurement of $d\chi/dE$. The spectral oscillation is a perfect registration of depth, since the oscillation comes from interferences, as shown in Fig. 2. Consequently, between n and $n+1$ oscillations, the data corresponds to a depth of n layers of GaSb plus $(n-1)$ layers of InAs, with an interval of pairs of InAs-GaSb layers. Therefore the oscillation of the random spectrum is a registration of depth independent of the projectile energy used in obtaining the spectrum.

To obtain the minimum channeling yield χ, we have to smooth the oscillations in the random and channeled spectra and evaluate χ at each node position by taking the ratio of the channeled spectrum to the random spectrum heights. For exam-

ple, in Fig. 11, $\chi(3)=22\%$ is located at the center of the third oscillation (slightly below 0.7 MeV of Fig. 11) and $\chi(4)=34\%$, $\chi(5)=46\%$. This gives an average of $d\chi/dx$ of 12% at the average depth 4, which is equivalent to the depth near the 3rd InAs and 4th GaSb interface (Fig. 2). The total layers above the 4th depth is between 6 to 7 layers depending on the amount of signal overlapping. The total thickness is (7)41 nm=287 nm. With a 45° tilt [near a ⟨110⟩ direction for a (100) crystal] this is equivalent to a depth of 287(1.414)=406 nm. In Fig. 11 the center of the 4th peak is located at 284 keV beneath the surface location, which results in a depth factor of 284 keV/406 nm=0.70 keV/nm. This is in good agreement with the calculated value of 0.68 keV/nm assuming Bragg's additivity and including in- and out-going energy losses at projectile energies around 1 MeV.

We have studied the dechanneling rate along the ⟨110⟩ direction on a (410,410 Å) superlattice sample at 1.0 MeV (Fig. 11), as well as at 1.5 MeV (Fig. 12), 2.0 MeV (Fig. 13), and 2.23 MeV (Fig. 9). The results are given in Table II. The minimum yields χ measured at three different depths x give values for $d\chi/dx$ at depth 4 of around 11−12% for all measurements. In this study our observation shows that the dechanneling is independent of the energy of the probing projectiles. The absence of an energy dependence for dechanneling indicates that the high ⟨110⟩ dechanneling is not caused by dislocations.

Channeling measurements have also been made on superlattices along the (110) planar direction

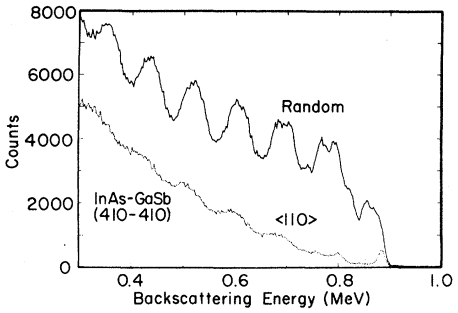

FIG. 11. Backscattering spectra for 1.01 MeV $^4He^+$ ions incident along a ⟨110⟩ direction in the same (410−410 Å) superlattice sample studied earlier, although the oscillatory nature is different due to difference in incident energy of the projectiles. The amount of dechanneling is very similar to that of Fig. 9.

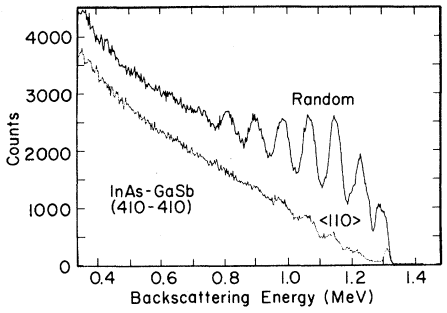

FIG. 12. Same as Fig. 11 except that the incident energy of the projectile is 1.50 MeV.

near a ⟨110⟩ axis; however, we did not find enhanced dechanneling. Axial channeling along a ⟨111⟩ direction on (100) superlattice samples also showed abnormally high dechanneling.

IV. INTERFACE MODEL

The absence of the energy dependence of the dechanneling (Table II) indicates that the high dechanneling rate along ⟨110⟩ directions on (100) superlattice samples is not due to defects of a dislocation nature. Campisano, Foti, Rimini, and Picraux[21] have shown that the amount of dechanneling is independent of ion-beam energy on crystal Si grown epitaxially on sapphire. Their transmission-electron-microscopy (TEM) micrographs indicate that Si grown on sapphire is loaded with stacking faults plus twin lammellac. The amount of dechanneling along ⟨110⟩ directions of the superlattices in our study is also independent of energy. This indicates that the defect observed

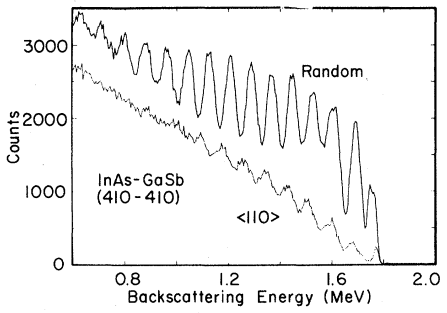

FIG. 13. Same as Fig. 11 except that the incident energy of the projectiles is 2.02 MeV.

TABLE II. ⟨110⟩ Dechanneling measurement.

Energy (MeV)	Depth Location	Minimum yield	$d\chi/dx$	$d\chi/dx$ (Av)
1.01	3	22%	12%	
(Fig. 11)	4	34%	12%	12%
	5	46%		
1.50	3	26%	13%	
(Fig. 12)	4	39%	11%	12%
	5	50%		
2.02	3	22%	12%	
(Fig. 13)	4	34%	10%	11%
	5	44%		
2.23	3	28%		
(Fig. 9)	4	38%	10%	11%
	5	50%	12%	

along ⟨110⟩ channeling directions are probably stacking faults.

The good channeling along the [100] growth direction for all superlattice samples studied is an indication that the assumed "stacking faults" are not observable along the [100] direction. A model which is consistent with our observations has been discussed briefly.[11] The basic features of this preferred model are illustrated in Fig. 14 by a side view of a thin InAs-layer sandwiched between two GaSb-layers. The thickness of the layers is irrelevant at this point. The InAs bond length is 0.2623 nm and that of GaSb is 0.2639 nm, a difference of only 0.7%. At each interface, however, the bond lengths are 7% different from the superlattice due to the fact that the InSb bond length is 0.2805 nm and the GaAs bond length is 0.2448 nm assuming InSb and GaAs solids. If we assume that these differences in bond lengths at the interfaces will lead to relaxation and contraction along the [100] direction, such as the simple model given in Fig. 14, then a higher dechanneling will occur due to the kink in the atomic strings at each interface along ⟨110⟩ directions but not along the [100] direction.

The total amount of dechanneling along ⟨110⟩ will be the composite effect of dechanneling due to three effects, such that it will produce a minimum yield χ_{tot} which is a function of depth, with the following relation:

$$(1-\chi_{\text{tot}})=(1-\chi_s)(1-\chi_d)(1-\chi_I)^N . \quad (1)$$

The first factor is due to the amount of dechanneling from a perfect single crystal due to the scattering from the surface layer and from atoms inside the crystal. We assign a constant $\chi_s=5\%$ based on the dashed curve of Fig. 9. We will ignore the depth dependence of χ_s.

The second factor is due to dechanneling from defects in the crystal. Based on Fig. 1, we assume that the amount of detectable defects in our superlattice are negligible from the dechanneling point of view, therefore, $\chi_d=0$, and Eq. (1) becomes

$$(1-\chi_{\text{tot}})=0.95(1-\chi_I)^N , \quad (2)$$

where χ_I is the minimum yield due to the scattering from interfacial kinks, such as those indicated schematically in Fig. 14. Here N is the number of interfaces which the ion beam passed at a given depth.

The value of χ_I is a strong function of the size of the kink displacement at the interface. The larger the kink displacement the larger the χ_I. Based on the model indicated in Fig. 14, for an ion beam directed along a ⟨100⟩ direction, there will be a kink in the atomic rows at each interface with a size of (7%) 0.26 nm=0.018 nm, protruding almost perpendicular to the row in the ⟨100⟩ directions.

The amount of dechanneling due to a kink of finite size has not been established in the past. However, dechanneling due to impurity atom displacements in a host crystal has been studied. For example, Picraux *et al.*[22] have measured and calculated the angular distribution of backscattering yield for Bi and Si when Bi atoms are displaced from the host lattice by a small distance. Their calculation indicates that a 0.02-nm displacement

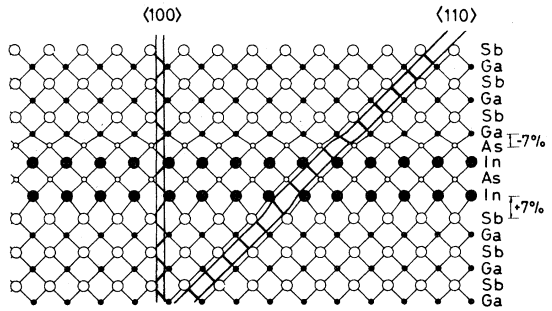

FIG. 14. Schematic diagram of a model for the InAs-GaSb superlattice. A 7% contraction at the Ga-As interface and a 7% relaxation at the In-Sb interface have no effect on the ion beam channeled along the [100] growth direction, but the contraction and relaxation produce kinks at the interfaces which obstruct the ion beam when channeled along a ⟨110⟩ direction.

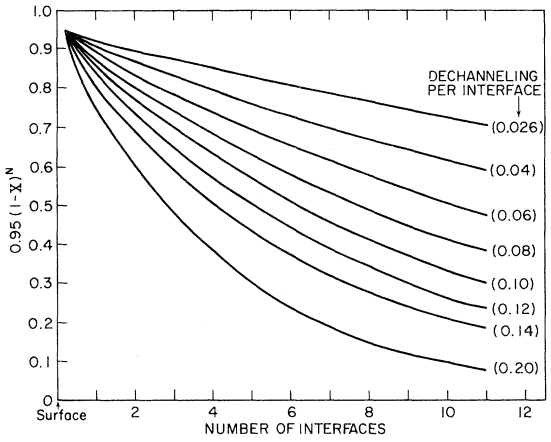

FIG. 15. Dechanneling due to interfacial displacements calculated based on Eq. (2), i.e., the amount of channeled beam versus number of interfaces for various dechanneling factors. This figure, when rotated 180° (reading it upside down), is correlated with the channeled ⟨110⟩ spectra shown on Figs. 9–12.

will cause a minimum increase in the yield χ of 2.6%.

The dechanneling calculation (Ref. 22) is for a single displaced atom, while the simple superlattice model (Fig. 14) is of an entire displaced string. It is difficult to justify the application of dechanneling calculation (Ref. 22) to the model (Fig. 14). Nevertheless, we have calculated the dechanneling based on Eq. (2) using 2.6% as the χ value. This result, as well as those for values of χ from 4% to 20%, are shown in Fig. 15. There are several interesting points we would like to make concerning these results. The number of interfaces N is also an expression of depth from the surface. The value $0.95\ (1-\chi)^N$ is the complementary of χ_{tot} based on Eq. (2). Therefore, if one turns Fig. 15 upside down, the figure becomes χ_{tot} versus negative depth which is directly related to the channeling yield versus backscattering energy. One can see the resemblance between the ⟨100⟩ channeled spectra given in Figs. 9–12 and that of Fig. 15, when the latter is turned upside down. It is very easy to convert the depth scale to the number of interfaces, or to the energy scale, since the oscillations give clear indications of both the location of the interfaces and of the number of layers involved.

For example, Fig. 9 shows that at the fifth peak, counting from the surface for the ⟨110⟩ spectrum χ_{tot} reaches 0.5. The fifth peak is equivalent to In_4-Sb_5 interface (see schematic spectrum of Fig. 2), and this interface is the 8th interface (see top of Fig. 2). At the eighth interface, Fig. 15 will intercept $1-\chi_{\text{tot}}=1-0.5=0.5$, on the 8% dechanneling curve. This means that we have 8% dechanneling per interface of χ_1 [of Eq. (2)] or $(1-0.08)^8 = 1-0.5$.

The value 8% is an estimated upper limit, since the dependence of depth of χ_s is ignored. The value of χ_1 at 8% is much higher than the 2.6% lower limit value calculated by the displacement mode.[22] Recent Monte Carlo computer simulations[23] of channeling in the superlattice also indicates that a 0.02-nm kink displacement at each interface can not account for the large amount of dechanneling observed experimentally.

The discrepancy discussed above can not be resolved easily. The model presented in Fig. 14 is conceptually simple and only qualitatively correct. The possible structural complexity at the interface is beyond the scope of this paper. Interdiffusion at the interface will smooth the kink into a slow transition region. Nevertheless, the intriguing fact is that very low dechanneling is expected along the [100] growth direction in this type of model.

V. SUMMARY

We have studied InAs-GaSb superlattices by Rutherford backscattering and channeling. A marked oscillatory structure in the backscattered spectrum confirms the superlattice periodicity.

Abnormally high dechanneling yield along ⟨110⟩ directions compared to the [100] growth

direction are observed. The channeling study was made as a function of layer thickness of the superlattice as well as a function of energy of the probing ion. The observations indicate that the high dechanneling along ⟨110⟩ directions is not caused by dislocations, but rather by a defect akin to stacking faults which are transparent to observations along the [100] growth direction. A simple calculation based on this model agrees qualitatively but not quantitatively with the experimental result. This discrepancy has not yet been resolved.

ACKNOWLEDGMENTS

We would like to express our thanks to J. F. Ziegler for the use of both the experimental facilities and the backscattering simulation programs, and to J. H. Barrett and L. L. Chang for stimulating discussions. The work was sponsored in part by the U. S. Army Research Office. Frans W. Saris would like to thank his colleagues at IBM for the warm hospitality extended to him.

[1]L. Esaki and R. Tsu, IBM J. Res. Dev. 14, 61 (1970).
[2]A. Y. Cho and J. R. Arthur, in *Progress in Solid State Chemistry,* edited by G. A. Somorjai and J. McCaldin (Pergamon, New York, 1975), Vol. 10, p. 157.
[3]L. L. Chang and R. Ludeke, in *Epitaxial Growth,* edited by J. W. Matthews (Academic, New York, 1975), Part A, p. 37.
[4]A. Y. Cho, Appl. Phys. Lett. 19, 467 (1971).
[5]L. L. Chang, L. Esaki, W. E. Howard, R. Ludeke, and G. Schul, J. Vac. Sci. Technol. 10, 655 (1973).
[6]L. L. Chang, Surf. Sci. 73, 226 (1978).
[7]C. A. Chang, R. Ludeke, L. L. Chang, and L. Esaki, Appl. Phys. Lett. 31, 759 (1977).
[8]L. L. Chang and L. Esaki, in *Progress in Crystal Growth and Characterization, 1979,* edited by P. Pamplin (Pergamon, London, 1979), Vol. 2, p. 3–14.
[9]R. Ludeke, L. Esaki, and L. L. Chang, Appl. Phys. Lett. 24, 417 (1974).
[10]J. W. Mayer, J. F. Ziegler, L. L. Chang, R. Tsu, and L. Esaki, J. Appl. Phys. 44, 2322 (1973).
[11]F. W. Saris, W. K. Chu, C. A. Chang, R. Ludeke, and L. Esaki, Appl. Phys. Lett. 37, 931 (1980).
[12]C. A. Chang and A. Segmüller, J. Vac. Sci. Technol. 16, 285 (1979).
[13]W. K. Chu, J. W. Mayer, and M.-H. Nicolet, *Backscattering Spectrometry* (Academic, New York, 1978).
[14]W. K. Chu, J. W. Mayer, M.-H. Nicolet, T. M. Buck, G. Amset, and F. Eisen, Thin Solid Films 17, 1 (1973).
[15]J. F. Ziegler, *Helium Stopping Powers and Ranges in All Elemental Matter* (Pergamon, New York, 1970).
[16]J. F. Ziegler, R. F. Lever, and J. K. Hirvonen, in *Ion Beam Surface Layer Analysis,* edited by D. Meyer, G. Linker, and F. Kappeler (Plenum, New York, 1976).
[17]W. K. Chu, Phys. Rev. A 13, 2057 (1976).
[18]W. K. Chu, in *Ion Beam Handbook for Material Analysis,* edited by J. W. Mayer and E. Rimini (Academic, New York 1977).
[19]G. Foti, S. T. Picraux, and S. U. Campisano, in *Ion Implantation in Semiconductors 1976,* edited by F. Cernow, J. A. Broders, and D. K. Brice (Plenum, New York, 1977), p. 249.
[20]Y. Quere, Phys. Status Solidi 30, 713 (1968).
[21]S. U. Campisano, G. Foti, E. Rimini, and S. T. Picraux, Nucl. Instrum. Methods 149, 371 (1978).
[22]S. T. Picraux, W. L. Brown, and W. M. Gibson, Phys. Rev. B 6, 1382 (1972).
[23]J. H. Barrett, Appl. Phys. Lett. 40, 482 (1982).